Preparation, physico-biochemical characterization, and proteomic analysis of highly transparent corneal extracellular matrices for lamellar keratoplasty and tissue-engineered cornea construction

Yoshihide Hashimoto [a,*], Jun Negishi [a,b], Seiichi Funamoto [a], Tsuyoshi Kimura [a,c], Hisatoshi Kobayashi [a], Tetsuro Oshika [d], Akio Kishida [a,**]

[a] *Institute of Biomaterials and Bioengineering, Tokyo Medical and Dental University, 2-3-10 Kanda-Surugadai, Chiyoda-ku, Tokyo, 101-0062, Japan*
[b] *Department of Applied Biology, Faculty of Textile Science and Technology, Shinshu University, 3-15-1 Tokida, Ueda, Nagano, 386-8567, Japan*
[c] *Department of Biomedical Engineering, Faculty of Life Science, Toyo University, 48-1 Oka, Asaka-shi, Saitama, 351-8510, Japan*
[d] *Department of Ophthalmology, Faculty of Medicine, University of Tsukuba, 1-1-1 Tennoudai, Tsukuba, Ibaraki, 305-8575, Japan*

A B S T R A C T

Corneal opacity and deformation, which often require corneal transplantation for treatment, are among the leading causes of monocular blindness. To restore corneal clarity and integrity, there is a need for an artificial stroma that not only matches the transparency of donated human cornea but also effectively integrates to the corneal tissue. In this study, a transparent decellularized cornea was successfully developed using the high hydrostatic pressure method with processing conditions optimized for corneal decellularization. Biochemical analyses demonstrated the effective removal of cellular components from the transparent decellularized corneas, while preserving collagen and glycosaminoglycans. Proteome analysis also revealed that core matrisome and matrisome-associated proteins remained following decellularization, similar to the composition observed in untreated corneas. The light transmittance of the transparent decellularized corneas was 86.4 ± 1.5 % in the visible region, comparable to that of donated human corneas. No complications, such as angiogenesis, were observed following interlamellar corneal transplantation in rabbits. The grafts were almost imperceptible immediately following surgery and achieved complete transparency within a few days, becoming indistinguishable even under a microscope. The transparent decellularized cornea presented here has promising potential as a material for application in lamellar keratoplasty.

1. Introduction

The cornea is an optically transparent and avascular tissue, which maintains its integrity through various factors derived from the tear film and aqueous humor [1]. It is primarily composed of three layers: a stratified epithelial layer on the anterior surface, a thick stromal layer composed of regularly arranged collagen fibrils interspersed with sparsely distributed interconnected keratocytes, and a monocellular endothelial layer. The corneal cells, along with a regular arrangement of collagen lamellae and proteoglycans, facilitate the maintenance of transparency within the extracellular matrix (ECM) [2]. However, diseases and injuries can damage the cornea, resulting in an irreversible loss of optical quality that ultimately leads to blindness [3].

Corneal transplantation using grafts from donor human corneas remains the gold standard treatment for many corneal disorders that lead to blindness. However, in many countries, the demand for donor corneas surpasses the available supply due to cultural and religious barriers, as well as logistical challenges [4,5]. According to the latest report, India

and China tops the list of the number of patients awaiting corneal transplantation worldwide, estimated at approximately 7 million and 2 million, respectively [6]. Furthermore, China has one of the highest rates of blindness globally, with approximately 12 million cases and an annual increase of around 450,000 individuals [7]. In addition, the clinical application of corneal transplantation is limited by factors such as low-quality donor corneas and the risk of graft rejection. In high-risk cases, rejection episodes occur in 30%–60 % of grafts, with up to 70 % failing within 10 years despite the use of local or systemic immuno-suppressive therapy [8,9]. To address these challenges, researchers have explored hydrogel-based artificial corneal constructs as a potential solution. These constructs are designed to facilitate the induction of corneal cells and nerves, and to mimic the biological functions of human donor corneas when implanted as lamellar grafts [10–12]. Despite considerable effort, most corneal substitutes have not yet achieved satisfactory results due to various limitations, including insufficient suture strength and elasticity [13,14]. Consequently, decellularized porcine corneas have gained considerable attention as an alternative to

donated human corneas [15,16]. They possess sufficient mechanical strength to withstand suturing during corneal transplantation [17,18], and also exhibit good biocompatibility in both in vitro and in vivo environments [19]. Currently, there are two types of decellularized corneas prepared using detergents and one prepared through a combination of freeze-thawing and sonication that are approved for clinical use in China. However, according to a recent report, 12 patients (30.8 %) experienced graft failure within 12 months [20].

We have previously demonstrated that decellularized corneas prepared using a high hydrostatic pressure (HHP) method without detergents exhibit suitable mechanical properties for suturing, low immunogenicity, excellent histocompatibility, and effective remodeling in rabbit models [21–25]. However, while the decellularized cornea achieves near complete transparency following transplantation, the initial issue of poor transparency prior to transplantation remains a challenge that requires further improvement.

In this study, we first addressed the optimization of processing conditions for corneal decellularization using the HHP method, successfully preparing a transparent decellularized cornea that meets the requirements for a transplantable artificial cornea. We then characterized the proteome, thickness, swelling behavior, and optical properties of the transparent decellularized cornea. Finally, we assessed the biocompatibility of the transparent decellularized cornea through cell viability assays, repopulation with corneal endothelial cells, and inter-lamellar corneal transplantation in rabbits.

2. Materials and methods

2.1. Chemicals

Deoxyribonuclease I (DNase I) and Dispase II were purchased from Roche Diagnostics K.K (Tokyo, Japan). Magnesium chloride hexahydrate ($MgCl_2 \bullet 6H_2O$) and Proteinase K were purchased from Merck Millipore Corporation (Tokyo, Japan). Gentamicin was purchased from Biomedal S.L (Sevilla, Spain). Dextran was purchased from Tokyo Chemical Industry Co., Ltd. (Tokyo, Japan). L-Ascorbic acid 2-phosphate trisodium salt, sodium chloride (NaCl), and sodium dodecyl sulfate (SDS) were purchased from Fujifilm Wako Pure Chemical Corporation (Osaka, Japan). Glycerol, 2-amino-2-hydroxymethyl-1,3-propanediol hydrochloride solution (Tris-HCl) were purchased form Sigma-Aldrich (St. Louis, USA). Ethylenediamine-N,N,N′,N′-tetraacetic acid, disodium salt, dihydrate (EDTA-2Na), and Cell Counting Kit-8 were purchased from Dojindo Laboratories (Kumamoto, Japan). Medium 199 (M199), minimum essential medium alpha (MEMα), Quant-iT PicoGreen, Eagle's minimal essential medium (EMEM), Dulbecco's modified Eagle's medium/Ham's F12 nutrient mixture (DMEM/F12), phosphate-buffered saline (PBS), and penicillin-streptomycin (10,000 U/mL) were purchased from Thermo Fisher Scientific K.K. (Tokyo, Japan). Gentamicin sulfate and basic fibroblast growth factor (bFGF) were purchased from Lonza K.K. (Tokyo, Japan). Fetal bovine serum was purchased from Hyclone Laboratories, Inc. (Tokyo, Japan).

2.2. Preparation of transparent decellularized corneas

Fresh porcine eye globes were obtained from a local slaughterhouse (Tokyo Shibaura Zoki K.K., Tokyo, Japan) and used within 4 h postmortem. The epithelium was mechanically removed to enhance the diffusion of the washing solutions into the corneal stroma using a corneal scarifier. The corneas were excised from the eyes and washed in a solution composed of an equal volume mixture of M199 and MEMα (M199/MEMα) supplemented with 15 % glycerol. The corneas were then placed in a plastic bag, filled with M199/MEMα supplemented with 15 % glycerol and subjected to HHP at 600 MPa at 10 °C for 10 min using a cold isostatic pressure machine (Dr. CHEF, Kobelco, Hyogo, Japan). The pressurized corneas were washed by continuous shaking in M199/MEMα supplemented with 0.2 mg/mL DNase I, 25 mM $MgCl_2 \bullet 6H_2O$,

0.5 mg/mL L-ascorbic acid 2-phosphate trisodium salt, 50 μg/mL gentamicin, and 35 mg/mL dextran at 25 °C for 3 days. This was followed by continuous shaking in a dextran solution at 4 °C for 1 day.

2.3. Histological evaluation

The untreated and transparent decellularized corneas were fixed in 4 % paraformaldehyde at room temperature for 24 h. They were then stepwise dehydrated using a series of 70%–100 % ethanol, then immersed in xylene, and embedded in paraffin. Subsequently, 4 μm sections were obtained, deparaffinized, and stained with hematoxylin and eosin (H-E) and Alcian blue. The sections were examined using an optical microscope equipped with a digital camera (BZ-X700; Keyence, Tokyo, Japan).

2.4. Immunohistochemistry

To prepare samples for immunocytochemical analysis, 5 μm thick sections were deparaffinized and treated with proteinase K or citric acid to achieve antigen retrieval. Following inactivation of endogenous peroxidase with 3 % hydrogen peroxide and blocking, the sections were incubated with the following primary antibodies: anti-human type I collagen antibody (dilution 1:100; Southern Biotech, AL, USA), anti-human type IV collagen antibody (dilution 1:200; Southern Biotech, AL, USA), anti-human vimentin antibody (V9; ready-to-use, Nichirei biosciences, Tokyo, Japan), anti-rabbit macrophage (CD68) antibody (RAM11; dilution 1:400, Dako Japan, Tokyo, Japan), anti-human smooth muscle actin antibody (1A4; dilution 1:400, Dako Japan, Tokyo, Japan), and anti-alpha-Gal epitope (Galα1-3Galβ1-4GlcNAc-R) antibody (M86; dilution 1:40, Enzo Life Sciences, NY, USA) at 4 °C overnight or at room temperature for 60 min. After washing with TBST (50 mM Tris-HCl buffer containing 0.05 % Tween 20 and 150 mM NaCl), the sections were incubated with a secondary antibody (Histofine Simple Stain MAX-PO system, Nichirei biosciences, Tokyo, Japan) at room temperature for 30 min, followed by staining with 3, 3- diaminobenzidine tetrahydrochloride (DAB). The sections were then examined using an optical microscope equipped with a digital camera.

2.5. DNA quantification

The untreated and transparent decellularized corneas were freeze-dried and weighed (n = 5), then 10 mg of each sample was digested with proteinase-K (30 mAnson-U/mg) in 50 mM Tris-HCl, 25 mM EDTA-2Na, 100 mM NaCl, and 1 % SDS solution at 55 °C for 12 h. DNA extraction was performed using a phenol/chloroform/isoamyl alcohol (25:24:1 vol%) method, followed by ethanol precipitation with sodium chloride. The concentration of total nucleic acid (TNA) and double-stranded DNA (dsDNA) were determined using UV/Vis spectroscopy (NanoDrop 2000, Thermo Fisher Scientific K.K., Tokyo, Japan) at 260/280 nm and the PicoGreen assay, respectively. For the PicoGreen assay, PicoGreen reagent was added to the residual DNA solution, and the fluorescence intensity was measured using a multi-mode microplate reader (Cytation 5; BioTek, VT, USA) at an excitation wavelength of 480 nm and emission wavelength of 521 nm. The amount of residual DNA was estimated from a λDNA standard curve and then normalized by dividing by the dry weight of the tissue samples.

2.6. Glycosaminoglycan (GAG) quantification

The untreated and transparent decellularized freeze-dried corneas (10 mg; n = 5), were digested with papain (0.1 mg/mL, Sigma-Aldrich) in 0.2 M sodium phosphate buffer supplemented with 100 mM sodium acetate, 10 mM EDTA-2Na, and 5 mM cysteine-HCl at 65 °C for 3 h. GAG content was assessed using the 1,9-dimethylmethylene blue dye binding assay (Blyscan Glycosaminoglycan Assay Kit, Biocolor, Ltd. Carrickfergus, UK).

2.7. Collagen quantification

The untreated and transparent decellularized freeze-dried corneas (10 mg; n = 5) were hydrolyzed with 6N HCl at 100 °C overnight. After removing the HCl, each sample was dissolved in assay buffer supplemented with 22 mM citric acid, 146 mM sodium acetate, 85 mM sodium hydroxide, and 42 mM glacial acetic acid, and then reacted with 62 mM chloramine-T solution and Ehrlich's solution. The absorbance was measured at 550 nm using a microplate reader. The amount of collagen was estimated from an L-hydroxyproline standard curve, applying a conversion factor where 1 mg of L-hydroxyproline corresponds to 7.46 mg of collagen, and then normalized by dividing by the dry weight of the tissue samples.

2.8. TEM analysis

The untreated and transparent decellularized corneas were fixed with 2 % glutaraldehyde at 4 °C for 24 h and subsequently post-fixed in 2 % osmium tetraoxide for 2 h on ice. The samples were dehydrated in graded ethanol and embedded in epoxy resin. Ultrathin sections were obtained using an ultramicrotome and were stained with uranyl acetate for 15 min. The sections were observed by a transmission electron microscope (TEM) (JEM-1400Flash, JEOL, Tokyo, Japan) at 100 kV. The diameter and density of collagen fibrils were analyzed from five different TEM images by Image J (Ver. 1.54).

2.9. Proteomic analysis of the transparent decellularized cornea

ECM-derived proteins were extracted from approximately 20 mg of transparent decellularized cornea. The protein concentration was quantified using a BCA assay, then cysteine residue alkylation was performed, followed by peptide fragmentation using trypsin/Lys-C Mix Mass Spec Grade (Promega, Tokyo, Japan). The purified peptide sample was reconstituted in a solvent (water/acetonitrile (98:2 v/v), 0.1 % trifluoroacetate), and then injected into an UltiMate 3000 RSLCnano LC system equipped with a Q Exactive HF-X (LC-nano ESI-MS/MS system, Thermo Fisher Scientific). The sample was separated on a nano HPLC capillary column (75 μm × 120 mm, C18, 3 μm, Nikkyo Technos, Tokyo, Japan) using solvent A (water, 0.1 % formic acid) at a flow rate of 200 nL/min. The LC gradient ranged from 6 % to 70 % solvent B (water/acetonitrile (20:80 v/v)) for 30 min [26]. DIA-NN software version 1.8.1 was used for MS data analysis. Identified proteins were categorized using Matrisome DB 2.0 [27] and the percentages of total proteins were calculated.

2.10. Corneal thickness and swelling behavior

The central thickness of the untreated and transparent decellularized corneas was measured using an ultrasound pachymeter (SP-100, Tomey, Nagoya, Japan) with a velocity of 1640 m/s, along with a micrometer with 2 μm accuracy (CLM1-15QMX, Mitutoyo, Kanagawa, Japan) (n = 4). To enhance the precision of cornea thickness measurements at each time point, the mean of 8 readings per sample was recorded. Corneal swelling was calculated according to the following equation. (1):

$$\text{Corneal swelling (\%)} = \frac{\text{Corneal thickness after treatment}}{\text{Initial corneal thickness}} \times 100 \quad (1)$$

2.11. Light transmittance

The center portion of the untreated and transparent decellularized corneas were trephined to a diameter of 6 mm and placed in 96-well glass bottom plate. Absorbance spectra were recorded with a resolution of 1 nm over 8 scans at each point from 300 nm to 800 nm (Cytation 5; BioTek, VT, USA) (n = 5). Each sample was independently measured five times under similar conditions. Absorbance values were then converted to percentages of light transmittance, assuming no reflection, using the following equation (2):

$$\text{Light transmittance (\%)} = 10^{(2-A)} \quad (2)$$

where A denotes the absorbance. The transparency of the cornea was estimated based on the average light transmittance across the range of 380–770 nm.

2.12. Refractive index

The refractive index of the transparent decellularized cornea was measured using a refractive index measurement system (Metricon Model 2010/M Prism Coupler, Metricon, NJ, USA) at 25 °C (n = 5). The samples were brought into contact with the prism base using a pneumatically operated coupling head. The angle of incidence of the laser beam can be adjusted using a rotary stage which accommodates the prism, waveguide, coupling head, and photodetector. The refractive index is determined by measuring the critical angle (θ_c) for the sample/prism interface. The wavelength used for measurements was 633 nm.

2.13. Suture retention test

The suture retention test was conducted using a universal testing machine (Autograph AG-X, Shimadzu, Tokyo, Japan) (n = 10). The center portion of the transparent decellularized cornea was trephined to a diameter of 10 mm and its thickness was measured using a micrometer with 2 μm accuracy. A stainless-steel wire suture, with a diameter of 0.070–0.099 mm, was threaded through each sample 2 mm from the edge of the transparent decellularized cornea. Each sample was preloaded to 0.01 N before loading. The suture retention strength was measured at a crosshead speed of 10 mm/min until the suture tore through the transparent decellularized cornea. The maximum load sustained by the transparent decellularized cornea was recorded as the suture retention strength, measured in newtons (N).

2.14. Compression test

The compression test was conducted using a universal testing machine equipped with compression platens (n = 4). The center portion of the transparent decellularized cornea was trephined to a diameter of 10 mm and its thickness was measured using a micrometer with 2 μm accuracy. Each sample was placed on the lower compression platen and the upper compression platen was gradually lowered to the sample until giving a fixed load of 0.01 N. The samples were compressed to 100 % deformation at a crosshead speed of 0.1 mm/s. The elastic modulus was calculated from the linear part of the stress–strain curve.

2.15. Cell viability assay

Cell viability was assessed using the elution method following established standards [28]. The transparent decellularized cornea, 8 mm in diameter, was immersed in 1 mL of EMEM for 24 h at 37 °C. Subsequently, the conditioned medium was collected as a corneal extract. Mouse fibroblasts (L929 cells) were obtained from ATCC (Rockville, MD, U.S.A) and cultured in EMEM supplemented with 10 % FBS, penicillin (100 units/ml) and streptomycin (100 μg/mL). L929 cells were seeded into 96-well plates at a density of 5×10^3 cells/cm^2. Following a 24-h incubation at 37 °C, the medium was replaced with 100 μl of undiluted extract, and the cells were further incubated for 24 h at 37 °C in 5 % CO$_2$. The same procedure was followed using 15 % glycerol and 10 % dimethyl sulfoxide (DMSO) as negative controls, while cells not exposed to any extracts served as the positive control. Cell viability was evaluated using a WST-8 assay (Cell Counting Kit-8), following the manufacturer's instructions.
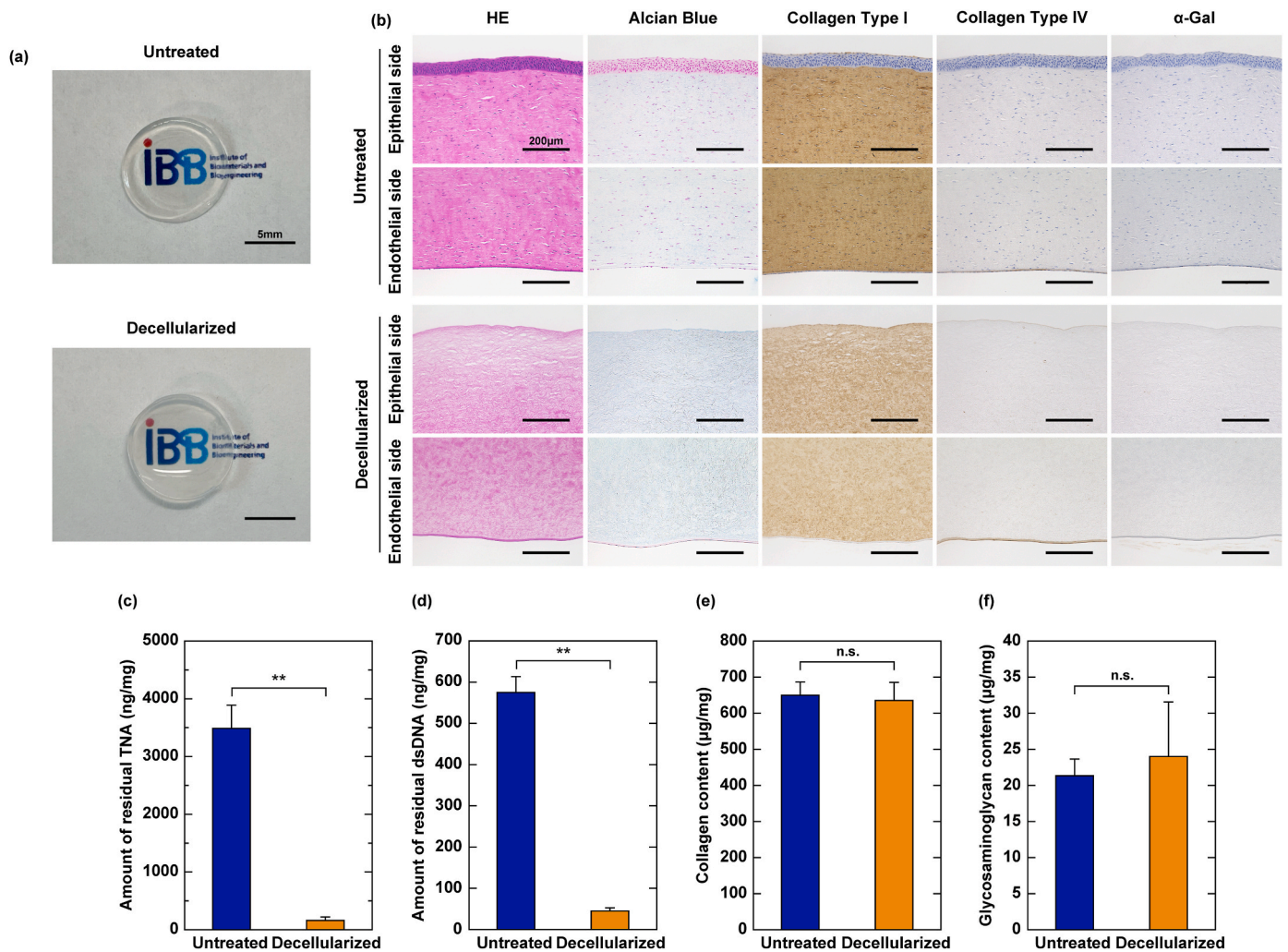
Fig. 1. Assessment of corneal decellularization using a modified high hydrostatic pressure method. (a) Macroscopic images of untreated and transparent decellularized corneas. Scale bars: 5 mm. (b) Histological and immunohistological analyses of untreated and transparent decellularized corneas. Scale bars: 200 μm. Quantitative analyses of (c) residual TNA, (d) residual dsDNA, (e) collagen content, and (f) GAG content in the untreated cornea and the transparent decellularized cornea, normalized to the dry tissue weight. Statistically significant differences are indicated by **$p < 0.001$ (n = 5).

2.16. Assessment of porcine corneal endothelial cell (PCEnC) repopulation

Fresh porcine eye globes were obtained within 4 h post-mortem from a local slaughterhouse (Tokyo Shibaura Zoki K.K., Tokyo, Japan) and disinfected using a 10 % isodine solution for 10 min. Following thorough washing in PBS containing 50 μg/mL gentamicin sulfate, the Descemet's membrane, including the corneal endothelium, was separated from the stroma under a stereomicroscope and then placed in a 35 mm culture dish containing 0.15 % dispase II (1.2 U/mL) in PBS. The tissue was incubated for 30 min at 37 °C, then the cells were detached by gentle pipetting. Cells were resuspended in DMEM/F12 supplemented with 10 ng/mL bFGF, 100 units/ml penicillin, 100 μg/mL streptomycin and 10 % FBS, then seeded onto a type IV collagen-coated 6-well culture plate. The culture medium was initially changed after 4 days, followed by subsequent changes every 2 days. Upon reaching confluence, the cells were seeded onto the transparent decellularized corneas at a density of 3000 cells/mm^2 and cultured for 7 and 14 days. Collagen gels were used as a control.

2.17. SEM analysis

The untreated and transparent decellularized corneas with

reconstituted endothelium were fixed with 2.5 % glutaraldehyde (TAAB Laboratories Equipment, Ltd., Berks, UK) in PBS for 24 h at 4 °C. Following dehydration using a gradient series of ethanol, each sample was immersed in t-butyl alcohol, and lyophilized. Subsequently, the lyophilized samples were coated with gold and observed using SEM with an accelerating voltage of 10 kV (S-3400NK, Hitachi High-Technologies Corp., Tokyo, Japan).

2.18. Interlamellar corneal transplantation

Male adult Japanese white rabbits (Kitayama Labes Co. Ltd., Nagano, Japan), aged 18 weeks and weighing 3.25 kg each, were used as the graft recipients. All animal procedures were conducted in accordance with the ARVO statement on the Use of Animals in Ophthalmic and Vision Research and were approved by the ethics committees for animal welfare of the Tokyo Medical and Dental University and the National Institutes for Materials Science. The transparent decellularized corneas were dissected to a thickness of 160 μm using a microkeratome (MK-2000, Nidek Co., Ltd., Tokyo, Japan). Recipient animals were anesthetized with sodium pentobarbital (35 mg/kg; Somnopentyl; Kyoritsu Seiyaku Corporation, Tokyo, Japan), and topical 0.4 % oxybuprocaine hydrochloride (Benoxil; Santen Pharmaceutical Co., Ltd., Osaka, Japan). The cornea was incised with a surgical knife to approximately half the
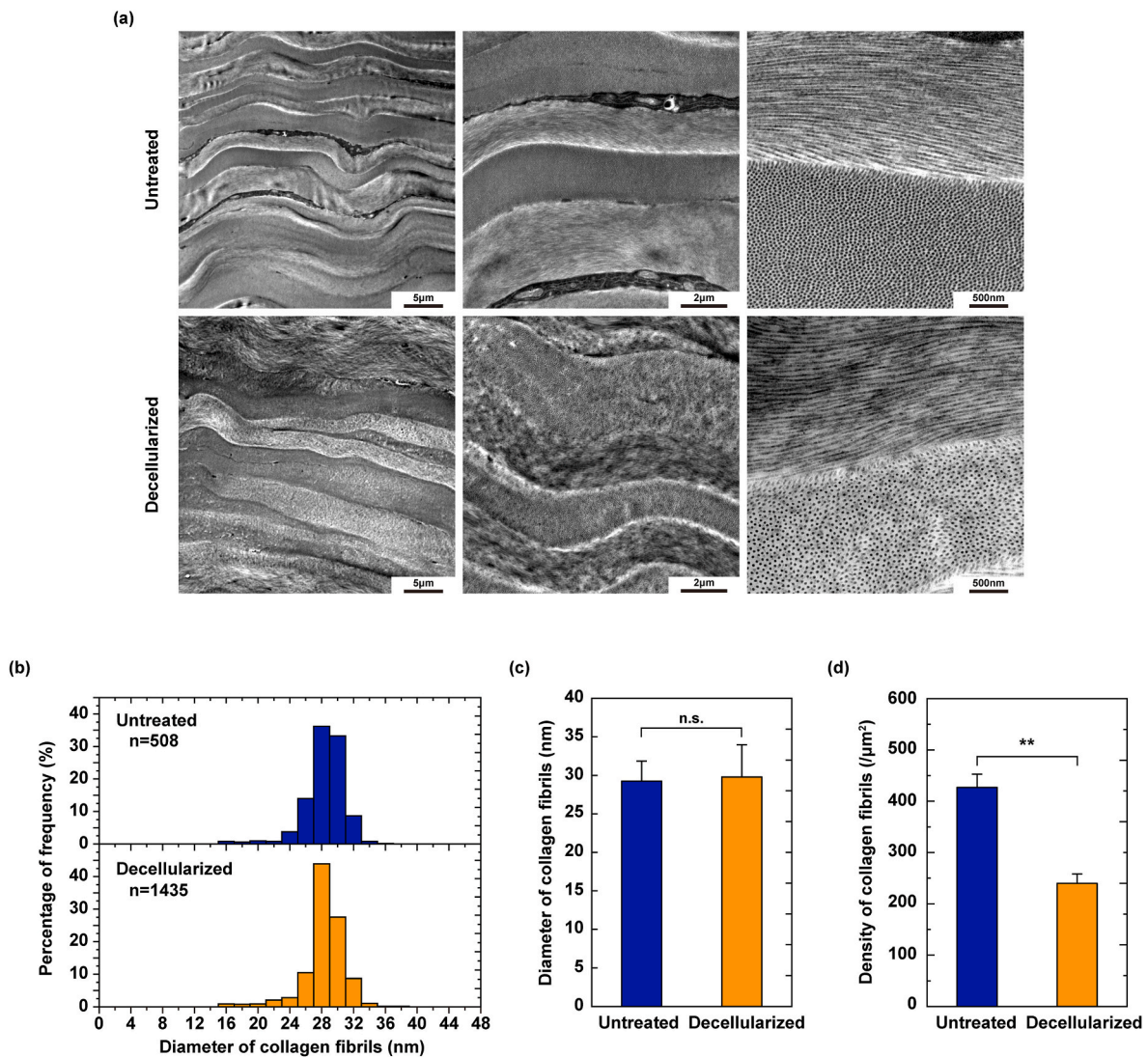
(a)

(b)   **(c)**   **(d)**

Fig. 2. Ultrastructural analysis of transparent decellularized corneas. (a) TEM images of horizontally arranged and vertically arranged collagen fibril layers in untreated and transparent decellularized corneas. (b) Histograms of the diameter distribution of collagen fibrils in untreated and transparent decellularized corneas. Quantitative analyses of (c) diameter of collagen fibrils, and (d) density of collagen fibrils in untreated and transparent decellularized corneas. Statistically significant differences are indicated by **$p < 0.001$ (n = 5).

depth of the corneal stroma at four positions 90° apart around the edge of the pupil (3, 6, 9, and 12 o'clock), and a corneal pocket was created with spatula. Transparent decellularized corneal discs (2 mm diameter) were inserted into the corneal pockets (n = 3). After 4 weeks, the rabbits were euthanized with an overdose injection of sodium pentobarbital. The rabbit corneas, including the samples, were excised and subjected to H-E and Masson's trichrome staining.

2.19. Statistical analysis

Data are presented as the mean ± standard deviation. Welch's *t*-test was used for comparisons of the DNA content. One-way analysis of variance (ANOVA), followed by Tukey's post hoc test were used for multiple group analysis and p < 0.05 was considered statistically significant. Significance levels for all tests were denoted as follows: *$p < 0.05$, and **$p < 0.001$.

3. Results

3.1. Optimization of hydrostatic pressure processing conditions for corneal decellularization

To investigate the effect of applied hydrostatic pressure on corneal transparency, hydrostatic pressure processing was applied in the range of 200 MPa–1000 MPa, and changes in corneal swelling and transmittance were measured. The swelling ratio was almost constant around 130 % regardless of the applied hydrostatic pressure, while the transmittance decreased drastically above 400 MPa (Figs. S1b and c). The effect of the pressure media on corneal transparency was investigated using M199/MEMα supplemented with varying concentrations of glycerol (0 %–30 %). The average thickness and transmittance of untreated corneas without epithelium were 774 ± 34 μm and 90.5 ± 3.8 %, respectively. When the corneas were immersed in M199/MEMα supplemented with glycerol, both the thickness and swelling ratio decreased, while the transmittance increased with higher glycerol concentrations (Fig. S1a). Based on achieving a balance between the swelling ratio and transmittance, the optimal glycerol concentration was determined to be 15 %, equal to 100 %, which is the swelling ratio of
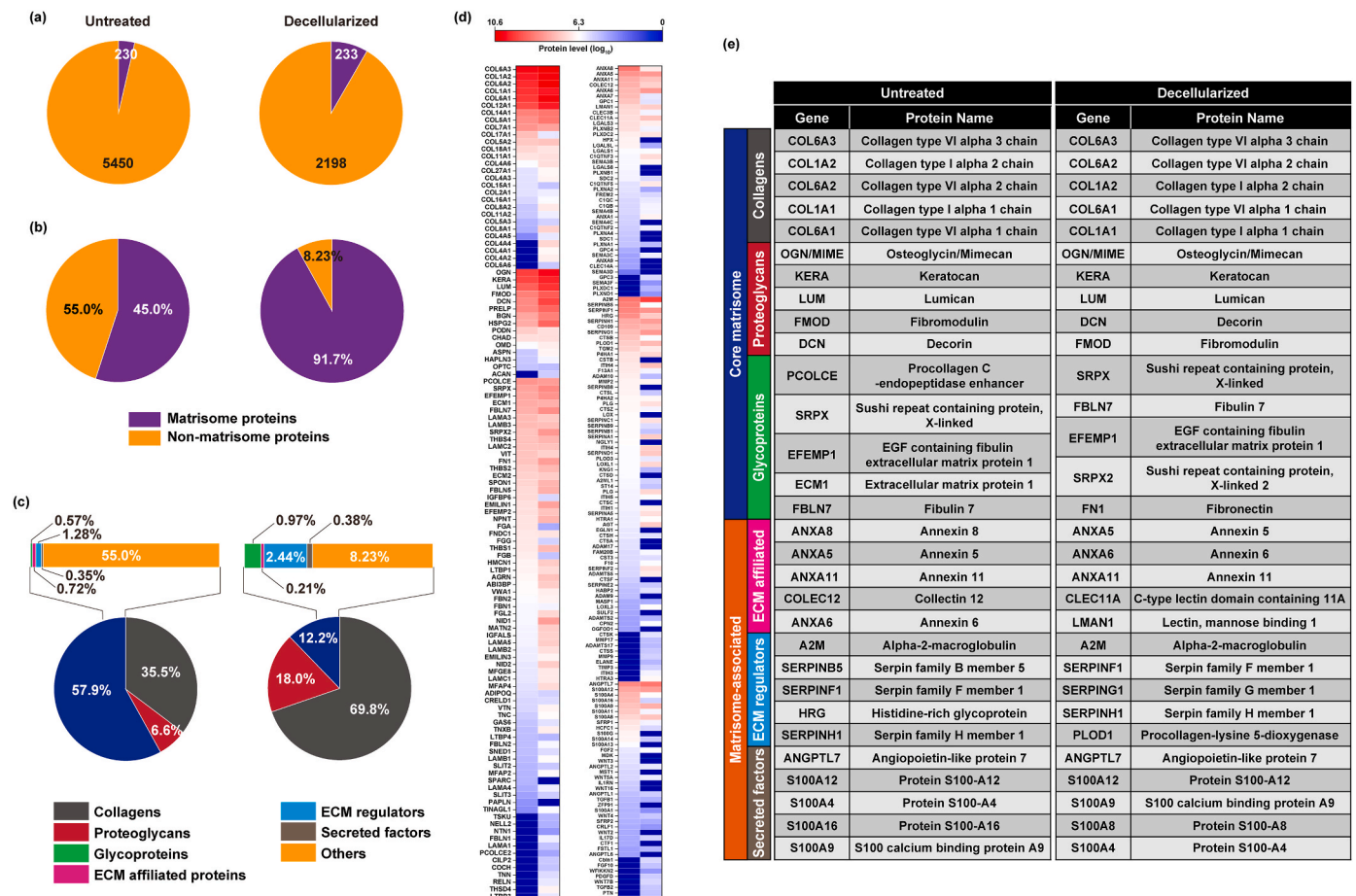
Fig. 3. Proteomic analysis of transparent decellularized corneas. (a) Total number of proteins identified by proteomics. (b) Percentage of matrisome proteins relative to total protein. (c) Composition of the matrisome protein subtypes as percentages. (d) Heat map displaying proteomic profiles. (e) The top 5 ECM components in the core matrisome and matrisome-associated proteins.

untreated corneas. Subsequently, changes in the swelling ratio and transmittance in corneas under different hydrostatic pressures were investigated in the presence of glycerol. The applied hydrostatic pressure had little effect on the swelling ratio (Fig. S1b); however, as the applied pressure increased, the transmittance decreased, with a sharp decrease observed above 600 MPa (Fig. S1c). The optimal glycerol concentration and applied hydrostatic pressure were determined to be 15 % and 600 MPa, respectively.

3.2. Preparation of transparent decellularized corneas

The macroscopic appearance of the transparent decellularized corneas remained unchanged even after the decellularization treatment, in contrast to the untreated porcine corneas (Fig. 1a). Histological and immunohistological analyses of the transparent decellularized corneas revealed the complete removal of corneal cells in each layer as a result of the modified HHP method, with no α-Gal epitope detected. Furthermore, the architecture of the stromal layers and their major components, including collagen type I and acidic mucopolysaccharides, were preserved. The integrity of the endothelial basement membrane, known as Descemet's membrane, was maintained after decellularization, as evidenced by collagen type IV staining (Fig. 1b). The efficacy of the decellularization process was assessed by quantifying TNA and dsDNA (Fig. 1c and d). The residual amounts of TNA and dsDNA were 3488.2 ± 400.8 ng/mg and 575.0 ± 38.7 ng/mg for untreated corneas, respectively, and 162.2 ± 59.4 ng/mg and 42.9 ± 7.3 ng/mg for transparent

decellularized corneas, respectively. Notably, both residual TNA and dsDNA levels after decellularization were significantly reduced by more than 93 % (n = 5, $p < 0.05$). The collagen content in untreated and transparent decellularized corneas was 650.0 ± 36.2 ng/mg and 635.3 ± 50.4 ng/mg (n = 5) respectively (Fig. 1e), while the GAG content was 21.3 ± 2.3 ng/mg and 24.0 ± 7.5 ng/mg (n = 5), respectively (Fig. 1f). There were no significant differences in either the collagen or sGAG content between untreated and transparent decellularized corneas.

3.3. Ultrastructural analyses of transparent decellularized corneas

The ultrastructure of transparent decellularized corneas was compared with that of the untreated corneas using TEM to define the impact of decellularization treatment using modified HHP method. The untreated cornea had highly ordered, stacked collagen layers called lamellae. The transparent decellularized cornea also maintained lamellar structure made of collagen fibrils and showed no noticeable structural changes (Fig. 2a). The average diameter of collagen fibrils was 29.3 ± 2.6 nm in untreated corneas and 29.8 ± 4.2 nm in transparent decellularized corneas, with no significant difference (Fig. 2b and c); however, the density of collagen fibrils was significantly different ($p < 0.001$). In transparent decellularized corneas, collagen fibrils were less dense and the interfibrillar spacing was wider than in untreated corneas (Fig. 2d).
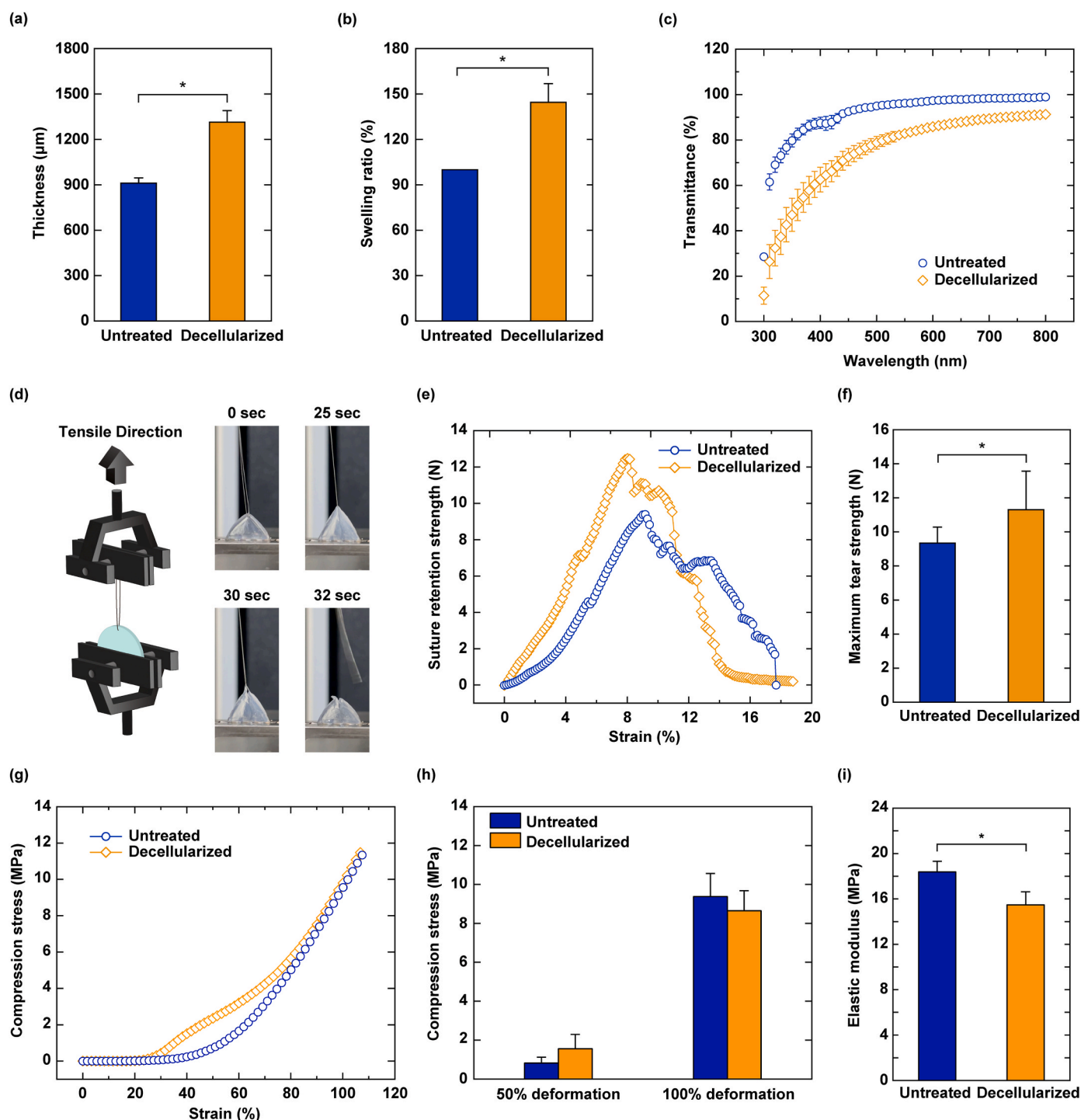
Fig. 4. Characterization of transparent decellularized corneas. (a) The thickness and (b) swelling ratio of transparent decellularized corneas. (c) The transmission spectra of untreated corneas (○) and transparent decellularized corneas (◇) for wavelengths ranging from 300 to 800 nm. (d) A schematic illustration of the suture retention testing and time-course changes of transparent decellularized corneas during loading. (e) Suture retention strength-strain curves of transparent decellularized corneas. (f) The maximum tear strength estimated from the suture retention strength-strain curves. (g) Compressive stress-strain curves of transparent decellularized corneas. (h) The stress at 50 % and 100 % deformation and (i) elastic modulus estimated from the compressive stress-strain curves. Statistically significant differences are indicated by *$p < 0.05$.

3.4. Proteome analysis of transparent decellularized corneas

Proteomic analysis of the transparent decellularized corneas identified a total of 2431 proteins, of which 233 were ECM components, constituting 91.7 % of all proteins detected. While the number of matrisome proteins remained largely unchanged before and after decellularization, the count of non-matrisome proteins decreased by less than half following the decellularization process (Fig. 3a and b). The classification of ECM components in the transparent decellularized corneas into core matrisome and matrisome-associated proteins, using the matrisome database, revealed that collagen, proteoglycan, and glycoproteins, constituting the core matrisome, accounted for 69.8 %, 18.0 %, and 0.97 % of the total, respectively. Matrisome-associated groups such as ECM-affiliated proteins, ECM regulators, and secreted factors,

Table 1

Comparison of key optical properties of the untreated corneas, transparent decellularized corneas, and fresh human corneas.

Sample	Transmittance [%]	Refractive index
Untreated porcine cornea	92.3 ± 1.2	1.375 ± 0.007
Transparent decellularized cornea	86.4 ± 1.5	1.367 ± 0.001
Fresh human cornea/(eye bank cornea)	87.1 ± 2.0[a)]/(62.5)[b)]	1.373–1.380[c)]

[a)] Transmittance at 500 nm [53].

[b)] Average transmittance of eye bank cornea measured at 450–650 nm in 50 nm increments [30].

[c)] The average refractive index of the stromal anterior and posterior surfaces of fresh human corneas [31].

accounted for 0.21 %, 2.44 %, and 0.38 % of the total, respectively. Decellularization resulted in a relative increase in the percentage of collagen and proteoglycans (Fig. 3c). Specifically, the top 5 collagens and proteoglycans of the core matrisome accounted for 92.1 % and 93.2 % of the total 28 collagens and 15 proteoglycans, respectively, found in the transparent decellularized corneas. In contrast, the top 5 glycoproteins within the core matrisome accounted for 47.7 % of the total 71 glycoproteins identified (Fig. 3d). Notably, there was minimal change in the top 5 core matrisome and matrisome-associated proteins before and after decellularization (Fig. 3e).

3.5. Characterization of the transparent decellularized corneas

The average thickness and swelling ratio of the transparent decellularized corneas were both approximately 1.4-fold greater than those of untreated cornea (n = 4, *p* > 0.05; Fig. 4a and b). The transmission spectrum of the transparent decellularized corneas was lower than that of the untreated cornea across all wavelengths in the range of 300–800 nm (Fig. 4c). The light transmittance, estimated from an average of 380–770 nm in the visible region, and the refractive index of each sample are summarized in Table 1. The transmittance of the untreated porcine corneas was 92.3 ± 1.2 % in the visible region. The light transmittance of transparent decellularized corneas was 86.4 ± 1.5 %, slightly lower than that of the untreated porcine cornea, but equivalent to that of the fresh human cornea (87.1 ± 2.0 %) [29], and greater than that of an eye bank preserved cornea [30]. The refractive index of the transparent decellularized corneas was 1.367 ± 0.001, which was slightly lower than that reported for human corneas at 1.373 to 1.380 [31].

The suture retention test demonstrated that both the untreated corneas and transparent decellularized corneas exhibited a rapid increase in the suture retention strength initially, followed by a gradual decrease after reaching the maximum value. The shape of the suture retention strength-strain curves is similar for both the untreated corneas and transparent decellularized corneas (Fig. 4d and e). The average maximum tear strength of the transparent decellularized corneas, as estimated from the suture retention strength-strain curves, was significantly higher than that of the untreated corneas (Fig. 4f). The compressive s-s curves of the transparent decellularized cornea showed a double sigmoid shape (Fig. 4g). There was no significant difference in stress at 50 % and 100 % deformation (Fig. 4h), but the elastic modulus was slightly lower than that of the untreated corneas (Fig. 4i).

3.6. Cell viability assay

Microscopic observations revealed that L929 cells cultured with the transparent decellularized corneal extracts adhered and proliferated normally (Fig. 5a). This suggests that the transparent decellularized corneal extracts did not induce changes in these cells compared with the positive control. Conversely, glycerol and DMSO, serving as negative controls, exhibited morphological changes and a decreased number of cells, indicating a highly toxic effect. The viability of L929 cells cultured

with the transparent decellularized corneal extracts was not significantly different from that of cells cultured with fresh medium (Fig. 5b). Glycerol and DMSO induced a significant decrease in cell viability compared with the positive control.

3.7. Recellularization of PCEnCs

PCEnCs were seeded onto the endothelial surface of the transparent decellularized corneas to assess its recellularization capacity. H-E staining revealed that PCEnCs adhered and covered the surface of the transparent decellularized cornea and collagen gels used as a control. A PCEnC monolayer, similar to the normal corneal endothelium, was maintained even after 1 and 2 weeks of culture. Descemet's membrane, the basement membrane of corneal endothelial cells, was reconstructed between the PCEnC monolayer and the transparent decellularized cornea, but not between the PCEnC monolayer and the collagen gel (Fig. 6a). DAPI staining demonstrated that PCEnCs sparsely adhered and gradually proliferated on the transparent decellularized cornea, while little proliferation was observed on collagen gels even though 2 weeks of culture after sparse adhesion (Fig. 6b). Although the cell density of PCEnCs on the transparent decellularized corneas after 1 and 2 weeks of culture was lower than that of the untreated corneas, a trend of increasing cell density with increasing culture period was observed (Fig. 6e). SEM observation also revealed that PCEnCs on the transparent decellularized corneas and the collagen gels reconstructed a confluent monolayer, with tight junctions observed between hexagonal shaped cells (Fig. 6c). The size of each individual cell was smallest in the untreated corneas, followed by the samples cultured for 2 weeks on the transparent decellularized corneas, the samples cultured for 1 weeks on the transparent decellularized corneas, and then the collagen gel (Fig. 6d). The percentage of regular hexagonal cells was lower in the corneal endothelium after 1 and 2 weeks of culture compared with the untreated corneal endothelium (Fig. 6f); however, the expression of Na⁺/K⁺-ATPase was detected by immunofluorescent staining of the corneal endothelium after 2 weeks of culture (Fig. 6g).

3.8. Interlamellar corneal transplantation

The transparent decellularized corneal matrix was transplanted into the interlamellar space of a rabbit corneal stroma to assess the biological responses elicited by xenotransplantation (Fig. 7a). There were no complications, including opacification and neovascularization, observed in any of the operated eyes for at least 4 weeks following surgery (Fig. 7b). The transparent decellularized corneal matrix was barely visible macroscopically immediately following surgery, with a haze score grade of 2 according to the grading system established by Fantes et al. [32]. It attained transparency within a maximum of 72 h and became indistinguishable from the rabbit cornea. This transparency was maintained during the postoperative follow-up, with an average haze score grade of 0.3 ± 0.29 (Fig. 7c). Histological sections of the implanted transparent decellularized corneal matrix 4 weeks following surgery are presented in Fig. 7e. H-E staining revealed the complete integration of the transparent decellularized corneal matrix with the rabbit stromal tissue. Moreover, a small number of keratocytes infiltrated into the graft as indicated by vimentin staining. Type I collagen staining demonstrated that there was no degradation or remodeling of the transparent decellularized corneal matrix. There were no α-SMA-positive cells observed within or around the transparent decellularized cornea; however, a small number of CD68-positive macrophages were observed surrounding it.

4. Discussion

Decellularized porcine cornea is being explored as a promising alternative for donated human corneas in lamellar keratoplasty [15,16], due to its many similarities in structure and composition of stromal
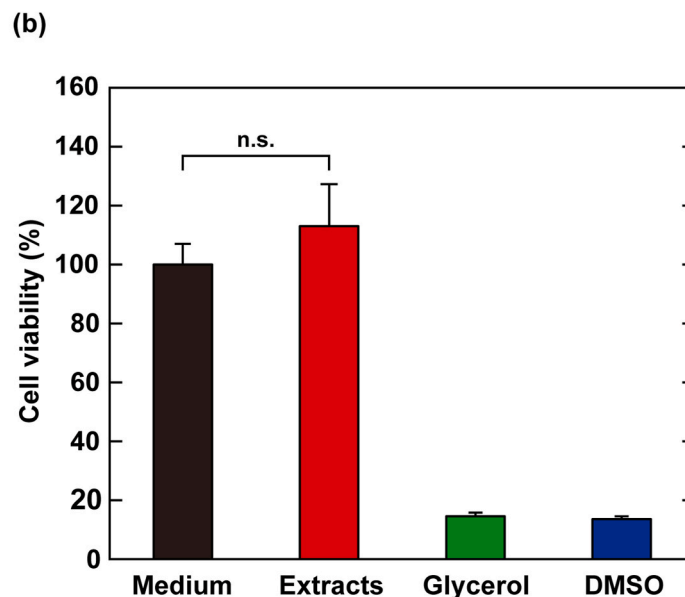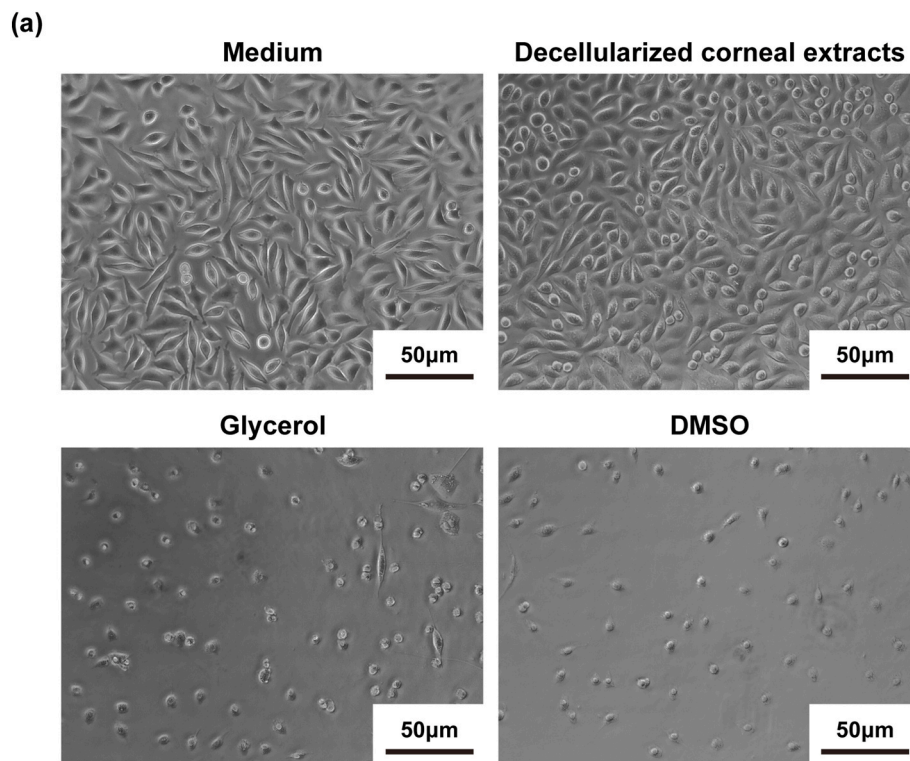
(a)

(b)

Fig. 5. Cell toxicity assessment using an extraction method. (a) Phase-contrast microscopy images of L929 cells after 24-h exposure to extracts from transparent decellularized corneas, glycerol, and DMSO. Scale bars: 50 μm. (b) Cell viability of L929 cells before and after exposure to each extract.

proteins [33,34]. To date, various decellularization techniques have been developed to reduce the xeno-immunogenicity of porcine corneas [35]. Three commercially available decellularized corneal products have been approved for clinical use by the National Medical Products Administration (NMPA) in China. While many decellularization techniques use detergents and hypertonic solutions, with or without nucleases, because they are simple and inexpensive [34], the use of chemical reagents can potentially disrupt the well-organized structure of the corneal stroma and limit biocompatibility due to cytotoxicity [36,37]. The removal of chemical reagents that can exhibit cytotoxic effects from the decellularized cornea is not only time-consuming [36,38], but can lead to a loss of mechanical properties and reduced transparency [39, 40]. The HHP method is a detergent-free physical decellularization technique, which has been previously demonstrated to yield a decellularized cornea with excellent in vivo biocompatibility [23–25]. The only drawback observed was a reduction in transparency of the decellularized cornea prepared by the HHP method prior to transplantation; however, this improves significantly post-implantation to achieve near transparency.

Corneal clarity is attributed to its lamellar structure, characterized by highly oriented and organized collagen nanofibers and proteoglycans, which are essential for maintaining structural integrity [2,
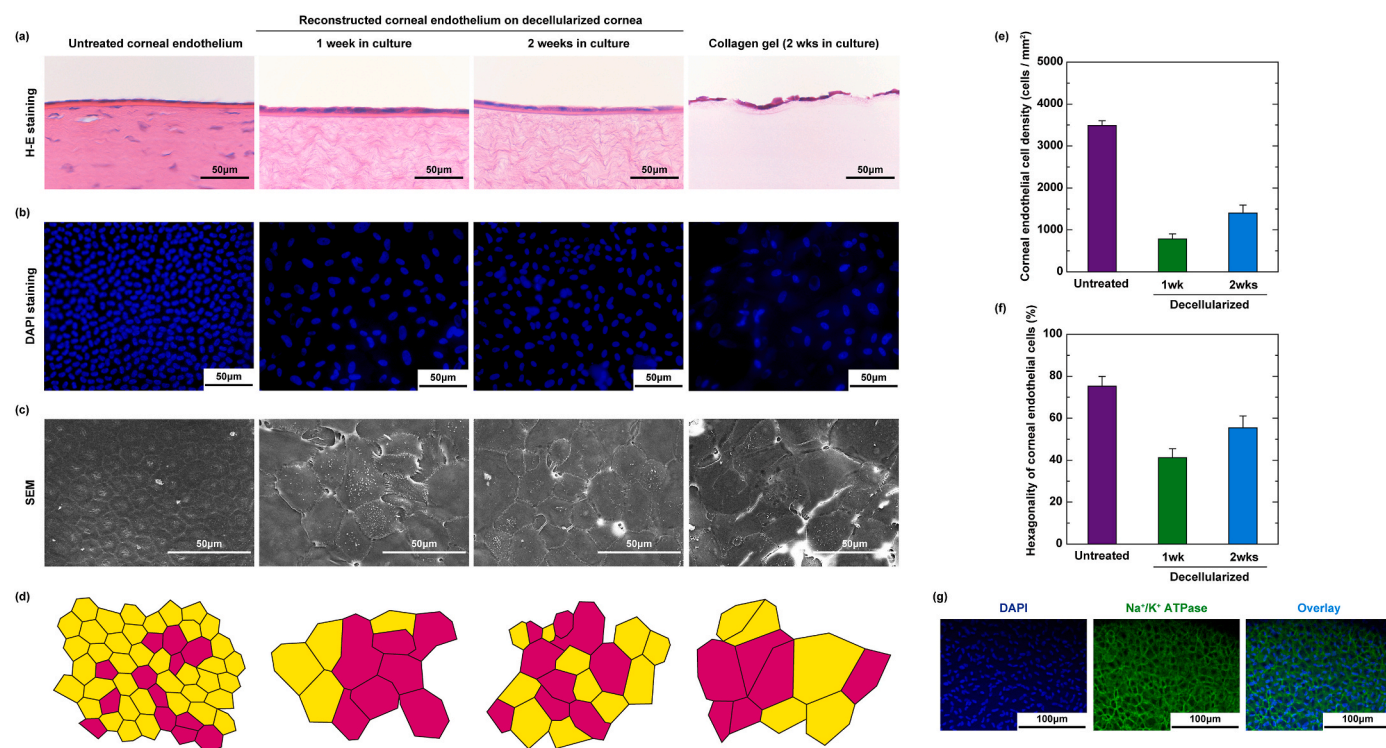
Fig. 6. Evaluation of corneal endothelial cell behavior on the transparent decellularized corneas. (a) H&E stained and (b) DAPI stained images of untreated corneas, transparent decellularized corneas with corneal endothelium cultured for 1 week, transparent decellularized corneas with corneal endothelium cultured for 2 weeks, and collagen gels with corneal endothelium cultured for 2 weeks. (c) SEM images of the corneal endothelium of the untreated corneas, corneal endothelium cultured on transparent decellularized corneas for 1 week, corneal endothelium cultured on transparent decellularized corneas for 2 weeks, and corneal endothelium cultured on collagen gels for 2 weeks and (d) their contour extraction images. (e) Corneal endothelial cell density calculated from cell nuclei staining images (n = 4). (f) Hexagonal morphology of corneal endothelial cells estimated from contour extraction images (n = 3). (g) Immunofluorescence staining of Na$^+$/K$^+$ ATPase in corneal endothelium cultured on decellularized corneas for 2 weeks. Nuclei were counterstained with DAPI.

41]. Therefore, any disruption to this lamellar structure or loss of proteoglycans not only comprises the transparency of the decellularized cornea, but also impacts its mechanical properties and refractive index. In this study, we aimed to refine the parameters of the HHP method, focusing on processing pressure and composition of the processing solution, to produce decellularized corneas with improved transparency. The concentration of glycerol in the pressure medium and the applied hydrostatic pressure were firstly optimized. Glycerol is known for its ability to significantly reduce tissue turbidity, and optical clearing effects have been reported in association with temporal tissue dehydration [42]. Glycerol also stabilizes the tertiary structure of collagen molecules through surface interactions [43,44]. The optimal glycerol concentration and applied hydrostatic pressure were determined to be 15 % and 600 MPa, respectively, based on the need for balance between the swelling ratio and transmittance (Fig. S1).

The protocols used to prepare decellularized tissues may affect both decellularization efficiency and ECM composition. Insufficient decellularization can induce strong inflammatory responses, while overly effective protocols for removing cellular components can inadvertently damage the ECM and remove various critical ECM components [45]. Therefore, striking a balance between effectively removing cellular components and preserving the integrity of the ECM structure is crucial. By using the modified HHP method, we achieved at least 93 % removal of TNA, with residual dsDNA levels below 50 ng/mg in porcine corneas. These levels meet the decellularization criteria proposed by Crapo et al. [46]. Furthermore, the quantities of major components such as collagen and GAG remained unchanged following decellularization, potentially contributing to the maintenance of transparency.

The diameter of collagen fibrils plays an important role in corneal transparency and is estimated to be in the range of 25–35 nm [47,48]. The diameter of collagen fibrils of transparent decellularized corneas

was consistent with that of untreated corneas and the literature values. On the other hand, the density of collagen fibrils in the transparent decellularized corneas found to be reduced to approximately two-thirds compared to that of the untreated corneas, which may be due to the swelling of the corneal stroma. Importantly, the lamellar structure made of collagen fibrils and transparency were preserved even after decellularization treatment, suggesting that the modified HHP method has little effect on tissue structure.

Through proteomic analysis, we conducted a comprehensive characterization of the transparent decellularized cornea. The top 5 proteins in both the core matrisome and matrisome-associated categories exhibited minimal change before and after decellularization, suggesting that the modified HHP method has little effect on ECM proteins. Significantly, key proteoglycans such as osteoglycin/mimecan, keratocan, lumican, and decorin, which play important roles in preserving corneal transparency, were identified [49,50]. Additionally, type VI collagen, which interacts with collagen fibrils via proteoglycan binding, stabilizes collagen fiber bundles, and contributes to their orderly arrangement, was also detected. Studies have demonstrated that type VI collagen not only facilitates cell migration and proliferation, suppresses apoptosis and oxidative damage, and regulates cell differentiation [51], but also modulates polarization toward anti-inflammatory macrophages and reduces the foreign body reaction [52]. These functions could potentially impact the in vivo performance of the decellularized cornea.

The visible light transmittance of the transparent decellularized cornea was comparable to that of previously reported human cornea [53], and higher than the average light transmittance at 450–650 nm of eye bank preserved human corneas reported by Rafat et al. [30]. This suggests that the transparency of the decellularized cornea meets the optical standards required for ocular applications, such as transplantable artificial corneas and corneal stroma substitutes. However, the
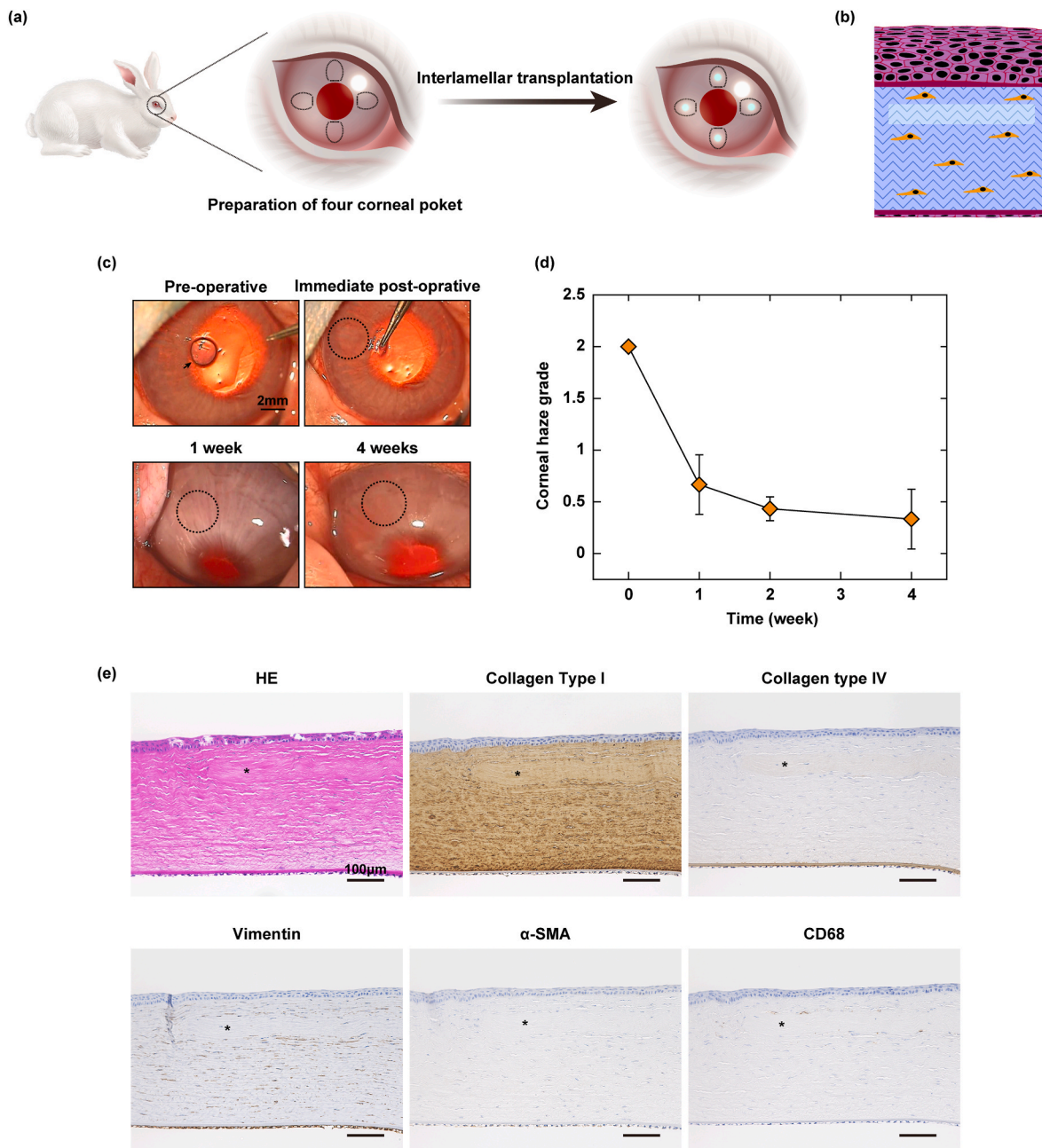
Fig. 7. In vivo assessment of transparent decellularized corneas using interlamellar keratoplasty. (a) Schematic illustration of interlamellar keratoplasty and (b) its cross-sectional image. (c) Representative macroscopic images of transparent decellularized corneas following transplantation. Scale bar: 2 mm. (d) Time-dependent changes in postoperative grades for transparent decellularized corneas (n = 3). (e) Representative histological sections of the transparent decellularized corneas at 4 weeks following surgery. The asterisk (*) represents implanted transparent decellularized corneas. Scale bar: 200 μm.

refractive index of the transparent decellularized cornea was slightly lower than that reported for both human cornea and porcine cornea. Corneal swelling tends to be more pronounced in the posterior region, a phenomenon attributed to structural differences along the axial direction of the stroma [54,55]. The anterior stroma typically exhibits lower hydration levels than the posterior stroma [56]. These hydration discrepancies between the anterior and posterior stroma contribute to alterations in the corneal stromal refractive index [57]. Thus, the lower refractive index observed in the transparent decellularized cornea may be a result of a higher swelling ratio compared with that of untreated corneal stroma.

The biological safety of the transparent decellularized corneas was assessed through cell viability assays using L929 cells exposed to corneal extracts. The in vitro experiments served as an initial screening step to

minimize animal-based testing. Glycerol and DMSO, typically used as cryo-protectant reagents for the long-term preservation of corneal tissue and cells [58,59], exhibited cytotoxic effects. Notably, the transparent decellularized corneal extracts facilitated normal proliferative activity, rather than any cytotoxic effects, on L929 cells. As revealed by the proteomic analysis, various bioactive substances remain within the transparent decellularized cornea, and these may have been released into the extract solution, potentially influencing cell proliferation.

Several reports have described the development of transparent decellularized corneas, primarily achieved by either thinly slicing the decellularized cornea or employing forced dehydration with high concentrations of glycerol to render the opaque corneas transparent following decellularization treatment [60]. However, the use of high concentrations of glycerol poses toxicity concerns, necessitating a

washing process before transplantation. During this washing process, the transparent decellularized cornea swells, once again becoming opaque. The most important aspect of this study is the retention of high transparency in the decellularized corneas developed herein, achieved without glycerol treatment post-decellularization. Therefore, these transparent decellularized corneas can be transplanted without the requirement of a washing process prior to transplantation.

Corneal endothelial cells (CEnCs) play an important role in maintaining corneal transparency. Damage or a significant decrease in CEnC density can lead to corneal edema and compromise transparency. Therefore, it is crucial to understand the behavior of CEnCs on the transparent decellularized corneas, particularly for expanding their potential clinical applications. In the normal adult human cornea, 60%–70 % of CEnCs exhibit a hexagonal shape [61], with an average cell density ranging from 2500 to 3000 cells/mm^2 [62]. In vivo, when CEnCs are damaged, neighboring cells often enlarge to compensate for the cell loss, resulting in a change of cell morphology from hexagonal to polygonal. Notably, within the first week of culture, primary PCEnCs seeded onto the transparent decellularized cornea successfully reconstructed the basement membrane. Over time, both cell density and hexagonality gradually increased. The absence of basement membrane reconstruction on the collagen gel suggests a potential influence of the surface structure or composition of the decellularized cornea.

The transparent decellularized cornea remained stable during xenogenic transplantation into a rabbit corneal stromal pocket, exhibiting no abnormal biological responses or changes in optical clarity, and successfully integrating with the surrounding tissues (Fig. 7). The stability observed was consistent with our previously reported findings on decellularized corneas [21,22,24]. This experiment confirmed the initial biological response to the transparent decellularized corneal matrix, with only a few CD68-positive macrophages observed. CD68 is known as a pan-macrophage marker, detecting both M1 pro-inflammatory macrophages and M2 anti-inflammatory macrophages [63]. The lack of inflammatory observations suggests that these macrophages may predominantly be of the M2 type. Therefore, it is plausible that the transparency observed after transplantation of the transparent decellularized corneas could be maintained for at least the 12 months that we have previously reported [22].

5. Conclusion

We have successfully developed a transparent decellularized cornea using a HHP method with processing conditions optimized for corneal decellularization. The transparent decellularized corneas exhibit high light transmittance in the visible region and a refractive index comparable to that of a donated human cornea, coupled with excellent biocompatibility. These effects were attributed to the retention of core matrisome components which are necessary to maintain the lamellar structure and transparency of the corneal stroma, as demonstrated by proteomic analysis. Taken together, these findings indicate that this transparent decellularized cornea holds promise as a material for lamellar keratoplasty as well as the in vitro expansion of corneal endothelial cells, offering new possibilities for developing artificial corneas.

CRediT authorship contribution statement

Yoshihide Hashimoto: Writing – review & editing, Writing – original draft, Supervision, Methodology, Investigation, Funding acquisition, Data curation, Conceptualization. **Jun Negishi:** Writing – review & editing, Methodology, Data curation. **Seiichi Funamoto:** Writing – review & editing, Methodology, Investigation, Data curation. **Tsuyoshi Kimura:** Methodology, Formal analysis, Data curation. **Hisatoshi Kobayashi:** Writing – review & editing, Supervision, Methodology, Investigation, Funding acquisition. **Tetsuro Oshika:** Writing – review & editing, Supervision, Methodology. **Akio Kishida:** Writing – review &

editing, Supervision, Project administration, Funding acquisition, Conceptualization.

Declaration of competing interest

The authors declare that they have no known competing financial interests or personal relationships that could have appeared to influence the work reported in this paper.

Data availability

Data will be made available on request.

Acknowledgements

Appendix A. Supplementary data

Supplementary data to this article can be found online at https://doi.org/10.1016/j.mtbio.2024.101241.

References

[1] K.M. Meek, C. Knupp, Corneal structure and transparency, Prog. Retin. Eye Res. 49 (2015) 1–16, https://doi.org/10.1016/j.preteyeres.2015.07.001.

[2] D. Massoudi, F. Malecaze, S.D. Galiacy, Collagens and proteoglycans of the cornea: importance in transparency and visual disorders, Cell Tissue Res. 363 (2) (2016) 337–349, https://doi.org/10.1007/s00441-015-2233-5.

[3] B. Barrientez, S.E. Nicholas, A. Whelchel, R. Sharif, J. Hjortdal, D. Karamichos, Corneal injury: clinical and molecular aspects, Exp. Eye Res. 186 (2019) 107709, https://doi.org/10.1016/j.exer.2019.107709.

[4] P. Gain, R. Jullienne, Z. He, M. Aldossary, S. Acquart, F. Cognasse, G. Thuret, Global survey of corneal transplantation and eye banking, JAMA Ophthalmol 134 (2) (2016) 167–173, https://doi.org/10.1001/jamaophthalmol.2015.4776.

[5] C.H. Yoon, H.J. Choi, M.K. Kim, Corneal xenotransplantation: where are we standing? Prog. Retin. Eye Res. 80 (2021) 100876 https://doi.org/10.1016/j.preteyeres.2020.100876.

[6] K.H. Wong, K.W. Kam, L.J. Chen, A.L. Young, Corneal blindness and current major treatment concern-graft scarcity, Int. J. Ophthalmol. 10 (7) (2017) 1154–1162, https://doi.org/10.18240/ijo.2017.07.21.

[7] L. Xie, Q. Zhou, H. Xu, P. Lin, The current situation of China's ophthalmology and visual science bioengineering, and a development strategy, Strateg Stud Chin Acad Eng 19 (2) (2017) 100–105, https://doi.org/10.15302/J-SSCAE-2017.02.017.

[8] T.B. Abud, A. Di Zazzo, A. Kheirkhah, R. Dana, Systemic immunomodulatory strategies in high-risk corneal transplantation, J. Ophthalmic Vis. Res. 12 (1) (2017) 81–92, https://doi.org/10.4103/2008-322X.200156.

[9] W.J. Armitage, C. Goodchild, M.D. Griffin, D.J. Gunn, J. Hjortdal, P. Lohan, C. C. Murphy, U. Pleyer, T. Ritter, D.M. Tole, B. Vabres, High-risk corneal transplantation: recent developments and future possibilities, Transplantation 103 (12) (2019) 2468–2478, https://doi.org/10.1097/TP.0000000000002938.

[10] P. Fagerholm, N.S. Lagali, J.A. Ong, K. Merrett, W.B. Jackson, J.W. Polarek, E. J. Suuronen, Y. Liu, I. Brunette, M. Griffith, Stable corneal regeneration four years after implantation of a cell-free recombinant human collagen scaffold, Biomaterials 35 (8) (2014) 2420–2427, https://doi.org/10.1016/j.biomaterials.2013.11.079.

[11] O. Buznyk, N. Pasyechnikova, M.M. Islam, S. Iakymenko, P. Fagerholm, M. Griffith, Bioengineered corneas grafted as alternatives to human donor corneas in three high-risk patients, Clin Transl Sci 8 (5) (2015) 558–562, https://doi.org/10.1111/cts.12293.

[12] M.M. Islam, O. Buznyk, J.C. Reddy, N. Pasyechnikova, E.I. Alarcon, S. Hayes, P. Lewis, P. Fagerholm, C. He, S. Iakymenko, W. Liu, K.M. Meek, V.S. Sangwan, M. Griffith, Biomaterials-enabled cornea regeneration in patients at high risk for rejection of donor tissue transplantation, NPJ Regen Med 3 (2018) 2, https://doi.org/10.1038/s41536-017-0038-8.

[13] V.S. De Stefano, W.J. Dupps, Biomechanical diagnostics of the cornea, Int. Ophthalmol. Clin. 57 (3) (2017) 75–86, https://doi.org/10.1097/IIO.0000000000000172.

[14] B. Kong, W. Sun, G. Chen, S. Tang, M. Li, Z. Shao, S. Mi, Tissue-engineered cornea constructed with compressed collagen and laser-perforated electrospun mat, Sci. Rep. 7 (1) (2017) 970, https://doi.org/10.1038/s41598-017-01072-0.

[15] M.C. Zhang, X. Liu, Y. Jin, D.L. Jiang, X.S. Wei, H.T. Xie, Lamellar keratoplasty treatment of fungal corneal ulcers with acellular porcine corneal stroma, Am. J. Transplant. 15 (4) (2015) 1068–1075, https://doi.org/10.1111/ajt.13096.

[16] W. Shi, Q. Zhou, H. Gao, S. Li, M. Dong, T. Wang, Y. Jia, C. Dong, X. Wang, Z. Guo, L. Zhao, X. Hu, L. Xie, Protectively decellularized porcine cornea versus human donor cornea for lamellar transplantation, Adv. Funct. Mater. 29 (37) (2019) 1902491, https://doi.org/10.1002/adfm.201902491.

[17] Y.H. Huang, F.W. Tseng, W.H. Chang, I.C. Peng, D.J. Hsieh, S.W. Wu, M.L. Yeh, Preparation of acellular scaffold for corneal tissue engineering by supercritical carbon dioxide extraction technology, Acta Biomater. 58 (2017) 238–243, https://doi.org/10.1016/j.actbio.2017.05.060.

[18] Q. Li, H. Wang, Z. Dai, Y. Cao, C. Jin, Preparation and biomechanical properties of an acellular porcine corneal stroma, Cornea 36 (11) (2017) 1343–1351, https://doi.org/10.1097/ICO.0000000000001319.

[19] M. Dong, L. Zhao, F. Wang, X. Hu, H. Li, T. Liu, Q. Zhou, W. Shi, Rapid porcine corneal decellularization through the use of sodium N-lauroyl glutamate and supernuclease, J. Tissue Eng. 10 (2019) 1–13, https://doi.org/10.1177/2041731419875876.

[20] S. Li, M. Li, L. Gu, L. Peng, Y. Deng, J. Zhong, B. Wang, Q. Wang, Y. Xiao, J. Yuan, Risk factors influencing survival of acellular porcine corneal stroma in infectious keratitis: a prospective clinical study, J. Transl. Med. 17 (1) (2019) 434, https://doi.org/10.1186/s12967-019-02192-z.

[21] S. Sasaki, S. Funamoto, Y. Hashimoto, T. Kimura, T. Honda, S. Hattori, H. Kobayashi, A. Kishida, M. Mochizuki, In vivo evaluation of a novel scaffold for artificial corneas prepared by using ultrahigh hydrostatic pressure to decellularize porcine corneas, Mol. Vis. 15 (2009) 2022–2028. http://www.molvis.org/molvis/v15/a216.

[22] Y. Hashimoto, S. Funamoto, S. Sasaki, T. Honda, S. Hattori, K. Nam, T. Kimura, M. Mochizuki, T. Fujisato, H. Kobayashi, A. Kishida, Preparation and characterization of decellularized cornea using high-hydrostatic pressurization for corneal tissue engineering, Biomaterials 31 (14) (2010) 3941–3948, https://doi.org/10.1016/j.biomaterials.2010.01.122.

[23] Y. Hashimoto, S. Funamoto, S. Sasaki, J. Negishi, T. Honda, S. Hattori, K. Nam, T. Kimura, M. Mochizuki, H. Kobayashi, A. Kishida, Corneal regeneration by deep anterior lamellar keratoplasty (DALK) using decellularized corneal matrix, PLoS One 10 (7) (2015) e0131989, https://doi.org/10.1371/journal.pone.0131989.

[24] Y. Hashimoto, S. Hattori, S. Sasaki, T. Honda, T. Kimura, S. Funamoto, H. Kobayashi, A. Kishida, Ultrastructural analysis of the decellularized cornea after interlamellar keratoplasty and microkeratome-assisted anterior lamellar keratoplasty in a rabbit model, Sci. Rep. 6 (2016) 27734, https://doi.org/10.1038/srep27734.

[25] Y. Hashimoto, S. Funamoto, S. Sasaki, J. Negishi, S. Hattori, T. Honda, T. Kimura, H. Kobayashi, A. Kishida, Re-epithelialization and remodeling of decellularized corneal matrix in a rabbit corneal epithelial wound model, Mater Sci Eng C Mater Biol Appl 102 (2019) 238–246, https://doi.org/10.1016/j.msec.2019.04.024.

[26] M. Ishikawa, R. Konno, D. Nakajima, M. Gotoh, K. Fukasawa, H. Sato, R. Nakamura, O. Ohara, Y. Kawashima, Optimization of ultrafast proteomics using an LC-quadrupole-orbitrap mass spectrometer with data-independent acquisition, J. Proteome Res. 21 (9) (2022) 2085–2093, https://doi.org/10.1021/acs.jproteome.2c00121.

[27] X. Shao, C.D. Gomez, N. Kapoor, J.M. Considine, C. Grams, Y.T. Gao, A. Naba, Matrisome DB 2.0: 2023 updates to the ECM-protein knowledge database, Nucleic Acids Res. 51 (D1) (2023) D1519–D1530, https://doi.org/10.1093/nar/gkac1009.

[28] J.L. Pariente, B.S. Kim, A. Atala, In vitro biocompatibility evaluation of naturally derived and synthetic biomaterials using normal human bladder smooth muscle cells, J. Urol. 167 (4) (2002) 1867–1871, https://doi.org/10.1016/S0022-5347(05)65251-2.

[29] E.M. Beems, J.A. Van Best, Light transmission of the cornea in whole human eyes, Exp. Eye Res. 50 (4) (1990) 393–395, https://doi.org/10.1016/0014-4835(90)90140-P.

[30] M. Rafat, F. Li, P. Fagerholm, N.S. Lagali, M.A. Watsky, R. Munger, T. Matsuura, M. Griffith, PEG-stabilized carbodiimide crosslinked collagen-chitosan hydrogels for corneal tissue engineering, Biomaterials 29 (29) (2008) 3960–3972, https://doi.org/10.1016/j.biomaterials.2008.06.017.

[31] S. Patel, J. Marshall, F.W. Fitzke, Refractive index of the human corneal epithelium and stroma, J. Refract. Surg. 11 (2) (1995) 100–105, https://doi.org/10.3928/1081-597X-19950301-09.

[32] F.E. Fantes, K.D. Hanna, G.O. Waring, Y. Pouliquen, K.P. Thompson, M. Savoldelli, Wound healing after excimer laser keratomileusis (photorefractive keratectomy) in monkeys, Arch. Ophthalmol. 108 (5) (1990) 665–675, https://doi.org/10.1001/archopht.1990.01070070051034.

[33] R. Sharifi, Y. Yang, Y. Adibnia, C.H. Dohlman, J. Chodosh, M. Gonzalez-Andrades, Finding an optimal corneal xenograft using comparative analysis of corneal matrix proteins across species, Sci. Rep. 9 (1) (2019) 1876, https://doi.org/10.1038/s41598-018-38342-4.

[34] M.M. Islam, R. Sharifi, S. Mamodaly, R. Islam, D. Nahra, D.B. Abusamra, P.C. Hui, Y. Adibnia, M. Goulamaly, E.I. Paschalis, A. Cruzat, J. Kong, P.H. Nilsson, P. Argüeso, T.E. Mollnes, J. Chodosh, C.H. Dohlman, M. Gonzalez-Andrades, Effects of gamma radiation sterilization on the structural and biological properties of decellularized corneal xenografts, Acta Biomater. 96 (2019) 330–344, https://doi.org/10.1016/j.actbio.2019.07.002.

[35] Y. Hashimoto, S. Funamoto, S. Sasaki, T. Kimura, H. Kobayashi, A. Kishida, Decellularized Matrix for Corneal Tissue Engineering: Recent Advances in Development and Clinical Potential, Decellularized Extracellular Matrix: Characterization, Fabrication and Applications, RSC Publishing, London, UK, 2019, pp. 219–236.

[36] S.L. Wilson, L.E. Sidney, S.E. Dunphy, H.S. Dua, A. Hopkinson, Corneal decellularization: a method of recycling unsuitable donor tissue for clinical translation? Curr. Eye Res. 41 (6) (2016) 769–782, https://doi.org/10.3109/02713683.2015.1062114.

[37] O. Syed, N.J. Walters, R.M. Day, H.W. Kim, J.C. Knowles, Evaluation of decellularization protocols for production of tubular small intestine submucosa scaffolds for use in oesophageal tissue engineering, Acta Biomater. 10 (12) (2014) 5043–5054, https://doi.org/10.1016/j.actbio.2014.08.024.

[38] N. Polisetti, A. Schmid, U. Schlötzer-Schrehardt, P. Maier, S.J. Lang, T. Steinberg, G. Schlunck, T. Reinhard, A decellularized human corneal scaffold for anterior corneal surface reconstruction, Sci. Rep. 11 (1) (2021) 2992, https://doi.org/10.1038/s41598-021-82678-3.

[39] A. Isidan, S. Liu, A.M. Chen, W. Zhang, P. Li, L.J. Smith, H. Hara, D.K.C. Cooper, B. Ekser, Comparison of porcine corneal decellularization methods and importance of preserving corneal limbus through decellularization, PLoS One 16 (3) (2021) e0243682, https://doi.org/10.1371/journal.pone.0243682.

[40] Q. Zheng, Y. Zhang, Y. Ren, Z. Zhao, S. Hua, J. Li, H. Wang, C. Ye, A.D. Kim, L. Wang, W. Chen, Deep anterior lamellar keratoplasty with cross-linked acellular porcine corneal stroma to manage fungal keratitis, Xenotransplantation 28 (2) (2021) e12655, https://doi.org/10.1111/xen.12655.

[41] T.J. Freegard, The physical basis of transparency of the normal cornea, Eye (Lond) 11 (Pt 4) (1997) 465–471, https://doi.org/10.1038/eye.1997.127.

[42] A.T. Yeh, J. Hirshburg, Molecular interactions of exogenous chemical agents with collagen–implications for tissue optical clearing, J. Biomed. Opt. 11 (1) (2006) 014003, https://doi.org/10.1117/1.2166381.

[43] K. Gekko, S. Koga, Increased thermal stability of collagen in the presence of sugars and polyols, J. Biochem. 94 (1) (1983) 199–205, https://doi.org/10.1093/oxfordjournals.jbchem.a134330.

[44] G.C. Na, Interaction of calf skin collagen with glycerol: linked function analysis, Biochemistry 25 (5) (1986) 967–973, https://doi.org/10.1021/bi00353a004.

[45] T.J. Keane, I.T. Swinehart, S.F. Badylak, Methods of tissue decellularization used for preparation of biologic scaffolds and in vivo relevance, Methods 84 (2015) 25–34, https://doi.org/10.1016/j.ymeth.2015.03.005.

[46] P.M. Crapo, T.W. Gilbert, S.F. Badylak, An overview of tissue and whole organ decellularization processes, Biomaterials 32 (12) (2011) 3233–3243, https://doi.org/10.1016/j.biomaterials.2011.01.057.

[47] L. Muthusubramaniam, L. Peng, T. Zaitseva, M. Paukshto, G.R. Martin, T.A. Desai, Collagen fibril diameter and alignment promote the quiescent keratocyte phenotype, J. Biomed. Mater. Res. 100 (3) (2012) 613–621, https://doi.org/10.1002/jbm.a.33284.

[48] S.K. Subasinghe, K.C. Ogbuehi, L. Mitchell, G.J. Dias, Animal model with structural similarity to human corneal collagen fibrillar arrangement, Anat. Sci. Int. 96 (2) (2021) 286–293, https://doi.org/10.1007/s12565-020-00590-8.

[49] M. Xuan, S. Wang, X. Liu, Y. He, Y. Li, Y. Zhang, Proteins of the corneal stroma: importance in visual function, Cell Tissue Res. 364 (1) (2016) 9–16, https://doi.org/10.1007/s00441-016-2372-3.

[50] E.M. Espana, D.E. Birk, Composition, structure and function of the corneal stroma, Exp. Eye Res. 198 (2020) 108137, https://doi.org/10.1016/j.exer.2020.108137.

[51] M. Cescon, F. Gattazzo, P. Chen, P. Bonaldo, Collagen VI at a glance, J. Cell Sci. 128 (19) (2015) 3525–3531, https://doi.org/10.1242/jcs.169748.

[52] A.C. Chen, W. Ciridon, S. Creason, B.D. Ratner, Surface immobilized α-1 acid glycoprotein and collagen VI modulate mouse macrophage polarization and reduce the foreign body capsule, J. Biomed. Mater. Res., Part A 112 (8) (2023) 1241–1249, https://doi.org/10.1002/jbm.a.37627.

[53] J. Doutch, A.J. Quantock, V.A. Smith, K.M. Meek, Light transmission in the human cornea as a function of position across the ocular surface: theoretical and experimental aspects, Biophys. J. 95 (11) (2008) 5092–5099, https://doi.org/10.1529/biophysj.108.132316.

[54] P. Erickson, T.L. Comstock, M.J. Doughty, A.P. Cullen, The cornea swells in the posterior direction under hydrogel contact lenses, Ophthalmic Physiol. Opt. 19 (6) (1999) 475–480, https://doi.org/10.1046/j.1475-1313.1999.00470.x.

[55] A.M. Moezzi, D. Fonn, T.L. Simpson, L. Sorbara, Contact lens-induced corneal swelling and surface changes measured with the Orbscan II corneal topographer, Optom. Vis. Sci. 81 (3) (2004) 189–193, https://doi.org/10.1097/00006324-200403000-00011.

[56] R. Turss, J. Friend, M. Reim, C.H. Dohlman, Glucose concentration and hydration of the corneal stroma, Ophthalmic Res. 2 (5) (1971) 253–260, https://doi.org/10.1159/000264570.

[57] I. Sanchez, R. Martin, F. Ussa, I. Fernandez-Bueno, The parameters of the porcine eyeball, Graefes Arch. Clin. Exp. Ophthalmol. 249 (4) (2011) 475–482, https://doi.org/10.1007/s00417-011-1617-9.

[58] N. Gupta, P. Upadhyay, Use of glycerol-preserved corneas for corneal transplants, Indian J. Ophthalmol. 65 (7) (2017) 569–573, https://doi.org/10.4103/ijo.IJO_56_17.

[59] S. Rodríguez-Fernández, M. Álvarez-Portela, E. Rendal-Vázquez, M. Piñeiro-Ramil, C. Sanjurjo-Rodríguez, R. Castro-Viñuelas, J. Sánchez-Ibáñez, I. Fuentes-Boquete, S. Díaz-Prado, Analysis of cryopreservation protocols and their harmful effects on the endothelial integrity of human corneas, Int. J. Mol. Sci. 22 (22) (2021) 12564, https://doi.org/10.3390/ijms222212564.

[60] X. Wang, A. Shakeel, A.E. Salih, H. Vurivi, S. Daoud, L. Desidery, R.L. Khan, M. G. Shibru, Z.M. Ali, H. Butt, V. Chan, P.R. Corridon, A scalable corneal xenograft platform: simultaneous opportunities for tissue engineering and circular economic sustainability by repurposing slaughterhouse waste, Front. Bioeng. Biotechnol. 11 (2023) 1133122, https://doi.org/10.3389/fbioe.2023.1133122.

[61] M. Ataş, S. Demircan, A.S. Karatepe Haşhaş, A. Gülhan, G. Zararsız, Comparison of corneal endothelial changes following phacoemulsification with transversal and torsional phacoemulsification machines, Int. J. Ophthalmol. 7 (5) (2014) 822–827, https://doi.org/10.3980/j.issn.2222-3959.2014.05.15.

[62] N. Okumura, Y. Sakamoto, K. Fujii, J. Kitano, S. Nakano, Y. Tsujimoto, S. Nakamura, M. Ueno, M. Hagiya, J. Hamuro, A. Matsuyama, S. Suzuki, T. Shiina, S. Kinoshita, N. Koizumi, Rho kinase inhibitor enables cell-based therapy for corneal endothelial dysfunction, Sci. Rep. 6 (2016) 26113, https://doi.org/10.1038/srep26113.

[63] H. Tian, J. Wu, M. Ma, Implications of macrophage polarization in corneal transplantation rejection, Transpl. Immunol. 64 (2021) 101353, https://doi.org/10.1016/j.trim.2020.101353.